Negative Differential Resistance in Graphene Boron Nitride Heterostructure Controlled by Twist and Phonon-Scattering

Yunqi Zhao, Zhenni Wan, Ulrich Hetmanuik, and M. P. Anantram

***Abstract*— The distinct negative differential resistance (NDR) mechanism arising from interlayer angular rotation in three-terminal graphene-BN heterostructures, as a function of both the twisting angle and the gate bias, is simulated and analyzed. Analytical expressions for the positions of the NDR peaks in the I–V characteristics are developed. To capture the degradation of peak-to-valley ratios observed in experiment at room temperature, electron–phonon scattering has been added to the simulation and good agreement with experiment is achieved. Our simulation also shows a robust preservation of NDR feature when temperature increases.**

***Index Terms*— Graphene heterostructure, Green's function, negative differential resistance, phonon scattering.**

I. Introduction

UNPRECEDENTED attention has been brought in 2D material over the past decades, leading to a variety of van de Waals heterostructures functionalized in both electrical [1]–[7] and optical [8]–[10] applications. Prototypical field-effect-transistor (FET) heterostructure devices based on graphene stacked with hexagonal boron nitride (hBN) [11], [12] or transitional metal dichalcogenides [4] have been recently realized experimentally. Among these heterostructures, a tunnel-FET device built with hBN vertically sandwiched by two graphene electrodes is of particular interest due to the observation of negative differential resistance (NDR). The appearance of NDR features in this multilayer tunnel-FET structure has the advantages of not requiring a bandgap opening in graphene and relatively simple fabrication process.

Recently, multiple theoretical works have focused on rationalizing the underlying physics of the NDR in graphene-hBN-graphene heterostructures [13]–[19]. Specifically, two distinct physical mechanisms are responsible for the NDR phenomenon [20], namely the Fabry-Pérot like quantum interference and the bias controlled Dirac cone alignment. These studies assume a perfect "AB" lattice structure between the hBN and graphene sheets. However, the lattice misorientation between stacked 2D atomic crystals is unavoidable during fabrication [12]. In this letter, by introducing a tunable angular misorientation between graphene and hBN layers, we investigate the transport properties for a twisted graphene-hBN-graphene device.

Manuscript received July 13, 2016; accepted July 24, 2016. Date of publication July 28, 2016; date of current version August 23, 2016. This work is supported by the National Science Foundation under Grant ECCS-1231927. The review of this letter was arranged by Editor J.-S. Moon.

Y. Zhao, Z. Wan, and M. P. Anantram are with the Department of Electrical Engineering, University of Washington, Seattle, WA 98195 USA (e-mail: zhaoyq@uw.edu).

U. Hetmanuik is with the Department of Applied Mathematics, University of Washington, Seattle, WA 98195 USA.

Color versions of one or more of the figures in this letter are available online at http://ieeexplore.ieee.org.

Digital Object Identifier 10.1109/LED.2016.2595522

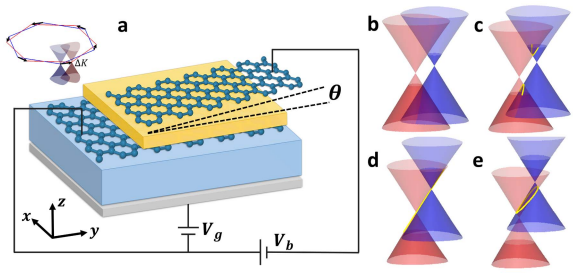


Fig. 1. (a) A schematic view of the twisted heterostructure device. An external gate electrode is applied on bottom graphene sheet. The top graphene layer is rotated with hBN insulator by an exaggerated angle θ. Inset: The Brillouin zones for bottom and top graphene layers in momentum space. The neutrality points of different graphene layers are displaced by ΔK. Oxide thickness $d_{OX} = 10nm$, and hBN thickness $d_{BN} = 0.66nm$. $\epsilon_{BN} = \epsilon_{OX} = 3.9$ (b)–(e): The horizontal distance between neutrality points is determined by the rotation angle θ and the vertical distance between them are determined by the applied gate voltage. (b) depicts the situation of $V_b = V_b^R$. (c)–(e) correspond to situations of $V_b < V_b^P$, $V_b = V_b^P$ and $V_b > V_b^P$. The red and blue cones represent the energy dispersions of bottom and top graphene layers respectively. Occupied and unoccupied states are distinguished by different transparency. The transmissive states that can carry tunnel current is highlighted by yellow curves.

II. Methods

The device [see Fig. 1(a)] consists of two semi-infinitely long monolayer armchair-edged graphene nanoribbon (AGNR) electrodes sandwiching a single layer hBN film as a tunneling barrier [11], [12]. An external gate electric field is applied vertically to the heterostructure. The quantum transport model here is different from [20] in two ways. The first is that the top graphene layer is rotated by a small tunable angle θ with respect to the central hBN. The sizes of the bottom AGNR and hBN sheets are 22.6nm (L_x along transverse direction) × 13.4nm (L_y along transport direction), and the size of the top AGNR sheet is 14.9nm × 13.4nm. The system Hamiltonian is constructed by considering a single p_z orbital for C, B and N atoms [21]. We adopt a Slater-Koster model [22] to capture the modulation of the interlayer hopping amplitude due to the lattice misorientation.

The second difference is the electrostatic model. Given the values of the bias voltage (V_b) and the gate voltage (V_g), the chemical potentials of top and bottom AGNR electrodes are determined by solving the following equations [23]:

$$\Delta\varphi_b + \mu_T - \mu_B = eV_b \quad (1)$$

$$\mu_B - \Delta\varphi_g = eV_g \quad (2)$$

In Eq. (1), $e = 1.6 \times 10^{-19}C$, and the first term $\Delta\varphi_b = e^2 d_{BN} n_T / \epsilon_{BN}$ is the electrostatic energy difference between

0741-3106 © 2016 IEEE. Personal use is permitted, but republication/redistribution requires IEEE permission.
See http://www.ieee.org/publications_standards/publications/rights/index.html for more information.

graphene electrodes (or equivalently the energy difference between two Dirac points). d_{BN} and ϵ_{BN} are the thickness and dielectric constant of hBN barrier. $n_{T(B)}$ is the difference in electron concentration in top (bottom) graphene sheet from charge neutrality. The second and third terms μ_T and μ_B are the chemical potentials of graphene electrodes defined by $\mu_{T(B)} = \pm\hbar v_F\sqrt{\pi\left|n_{T(B)}\right|}$ with v_F being the Fermi velocity of graphene. Note that the chemical potential in this letter is defined as the Fermi energy of graphene electrodes minus their respective Dirac points. In the Eq. (2), $\Delta\varphi_g = e^2 d_{OX} n_{ext}/\epsilon_{OX}$ is the electrostatic energy difference between bottom graphene and gate electrode. d_{OX} is the thickness of gate oxide. n_{ext} denotes the gate-induced charge density on gate electrode (typically n-Si), satisfying $n_B + n_T + n_{ext} = 0$.

The quantum transport is simulated by the *non-equilibrium Green's function* (NEGF) method [24]. The retarded Green's function and lesser (greater) Green's function are defined in:

$$\mathbf{A} = \varepsilon\mathbf{S} - \mathbf{H} - \mathbf{\Sigma}_C^r - \mathbf{\Sigma}_{ph}^r \tag{3}$$

$$\mathbf{G}^r = \mathbf{A}^{-1}, \mathbf{AG}^{<,>} = \left(\mathbf{\Sigma}_C^{<,>} + \mathbf{\Sigma}_{ph}^{<,>}\right)\mathbf{G}^A \tag{4}$$

Here, $\mathbf{S}$ and $\mathbf{H}$ are system overlap and Hamiltonian matrices. ε is the electron energy. $\mathbf{G}^A$ is the Hermitian of $\mathbf{G}^r$. Self-energy matrices $\mathbf{\Sigma}_C^{r,<,>}$ and $\mathbf{\Sigma}_{ph}^{r,<,>}$ represent the effect of contacts and electron-phonon scattering. Both source and drain contribute to contact self-energies $\mathbf{\Sigma}_C^{r,<,>} = \mathbf{\Sigma}_S^{r,<,>} + \mathbf{\Sigma}_D^{r,<,>}$. The evaluation of $\mathbf{\Sigma}_{S,D}^r$ are described in [24]. $\mathbf{\Sigma}_{S,D}^< = -2if_{S,D}\mathrm{Im}\left[\mathbf{\Sigma}_{S,D}^r\right]$, and $\mathbf{\Sigma}_{S,D}^> = 2i\left(1 - f_{S,D}\right)\mathrm{Im}\left[\mathbf{\Sigma}_{S,D}^r\right]$, where $f_{S,D}$ are the Fermi factors in the source and drain electrodes. The evaluation of $\mathbf{\Sigma}_{ph}^{r,<,>}$ will be discussed in later section when scattering is included. The current density is defined by

$$j\left(k,\varepsilon\right) = \frac{1}{2\pi}\mathrm{Tr}\left[\mathbf{T}_{k,k+1}\mathbf{G}_{k+1,k}^< - \mathbf{G}_{k+1,k}^<\mathbf{T}_{k,k+1}\right] \tag{5}$$

where $\mathbf{T} = \varepsilon\mathbf{S} - \mathbf{H}$; and k denotes k-th atomic layer along the transport direction. Instead of solving Green's function by the widely used recursive approach, a novel method, namely *HSC-extension* [25], enables us to efficiently perform the requisite large-scale calculations.

III. Results

A. Features of NDR Peaks

We start by analyzing the twisted device with zero external gate voltage. The simulated I-V curves, shown in Fig. 2, exhibit strong NDR peaks, whose location and peak current depends on the misalignment angles.

In the untwisted system ($\theta = 0$), the I-V curves in Fig. 2(a) show multiple current peaks which are fully induced by a Fabry-Pérot interference mechanism [20]. When θ deviates from perfect alignment and increases, the oscillations gradually disappear. We explain this quenching of current peaks at non-zero twisting angles by looking at the resonant condition of Fabry-Pérot like interference. In the case of perfect lattice alignment, the transmission states lie on a circular curve with wavevectors at the same energy. When the energy of these states satisfies the resonant condition for Fabry-Pérot interference, all states along the circular curve are capable of carrying current. However, the angular misorientation between

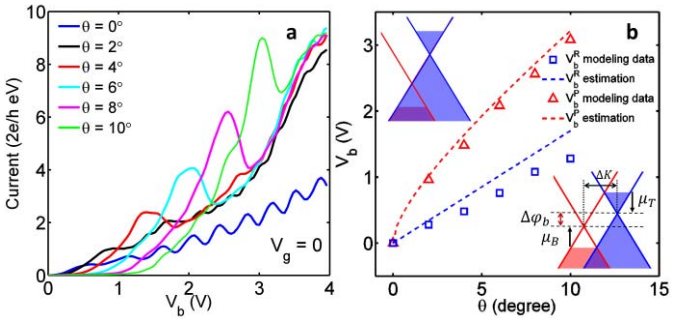


Fig. 2. (a) Calculated I-V curves for a family of twisting angle with $V_g = 0$. (b) V_b^R and V_b^P as a function of θ for both simulated results (markers) and analytical (dashed) estimations. Top inset: illustration of the situation at V_b^P, a 2D version of Fig. 1(d). Bottom inset: illustration of the situation at V_b^R where tunneling current begins to increase rapidly from zero, a 2D version of Fig. 1(b). The electrostatic model is defined in Eq. (1-2).

graphene layers creates a displacement between two Dirac cones in momentum space. As a result of the conic intersection, the transmission states lie on a hyperbolic [Fig. 1(c)] or elliptic [Fig. 1(e)] curve without sharing the same energy. Therefore, the number of transmissive states that can tunnel resonantly with the assistance of Fabry-Pérot like interference are greatly suppressed, leading to the damping of current oscillations.

At non-zero θ, the current is close to zero at small biases in Fig. 2(a), and the current rapidly grows after a particular bias voltage V_b^R. We explain this feature by depicting the conic dispersions of the two graphene layers at $V_b = V_b^R$ in Fig. 1(b). When $V_b < V_b^R$, although the Dirac cones intersect along a hyperbolic curve, all transmissive states are occupied in both top and bottom graphene layers, yielding a zero tunneling current. At $V_b = V_b^R$, the occupied/unoccupied states of the bottom (red)/top (blue) Dirac cones intersect only at two points shown in Fig. 1(b) [also shown in Fig. 2(b) bottom inset]. When $V_b > V_b^R$, a fraction of the states in the hyperbolic intersection is unoccupied at top layer [Fig. 1(c)], resulting in a rapid increase of current.

To explain how V_b^R changes as a function of θ, we provide a formula for V_b^R by solving Eq. (1-2) under the situation displayed in Fig. 1(b), that is $\Delta\varphi_b + \mu_T + \mu_T \sim \hbar v_F \Delta K$, where $\Delta K = \frac{4\pi}{3a}\theta$ we obtain that at small θ ($V_g = 0$):

$$V_b^R = \frac{\hbar v_F}{e}\Delta K = \frac{4\pi}{3a}\frac{\hbar v_F}{e}\theta \tag{6}$$

Next, as the source-drain bias becomes larger, strong NDR peaks occur at V_b^P, when the intersection between two Dirac cones becomes a straight line [23], [26]. V_b^P as a function of twisting angle can also be evaluated by solving Eq. (1-2) corresponding to Fig. 1(d) [see illustration in Fig. 2(b) inset], and using $\Delta\varphi_b = \hbar v_F \Delta K$, the value of V_b^P can be expressed as a function of θ:

$$V_b^P = \frac{\hbar v_F}{e}\Delta K + \frac{\left(\hbar v_F\right)^{3/2}}{e^2}\sqrt{\frac{\pi\epsilon_0\epsilon_{BN}}{d_{BN}}} \times\left(\sqrt{\Delta K} + \sqrt{\Delta K + \frac{d_{BN}}{d_{OX}}\left(\frac{\hbar v_F \pi\epsilon_0\epsilon_{BN}}{4e^2 d_{OX}} - \frac{eV_g}{\hbar v_F}\right)}\right) - \frac{\left(\hbar v_F\right)^2\pi\epsilon_0\epsilon_{BN}}{2e^3 d_{OX}} \tag{7}$$

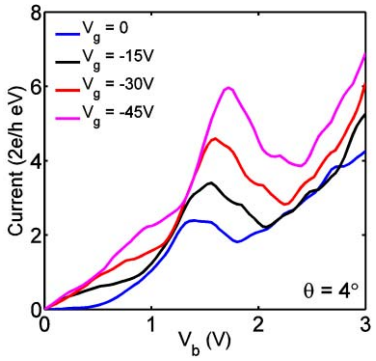


Fig. 3. Calculated I-V curves for a fixed non-zero twisting angle $\theta = 4°$ with various gate voltages.

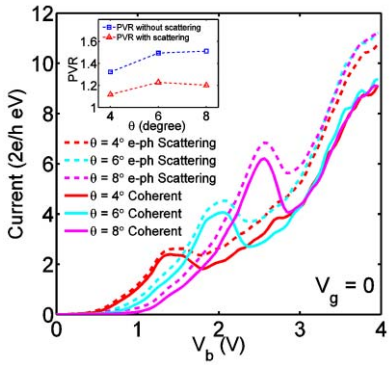


Fig. 4. Calculated I-V curves for a family of θ at $V_g = 0$with electron-phonon scattering (dashed curves). For comparison, the corresponding results of coherent transport [from Fig. 2(a)] are plotted as solid curves.

The estimations of V_b^R and V_b^P are compared against the simulated values in Fig. 2(b), indicating a quantitative match between the analytical formula and numerical results.

B. Gate Controllability

For a twisted heterostructure with fixed angle $\theta = 4°$, we model the current-voltage characteristics with various values of V_g in Fig. 3. Pronounced resonant peaks whose locations and amplitudes vary as a function of gate voltage are seen as the gate electrode modulates the electrostatic potentials by changing the carrier concentration in graphene layers. As a result, the gate electrode alters the energy difference between the Dirac points on the two sheets, thereby shifting the value of V_b^P. Our calculated dependence on V_g is qualitatively consistent with experimental results in [12].

C. Impact of Phonon Scattering

According to [12] when the environmental temperature increases from 2K to room temperature, the measured peak-to-valley ratio (PVR) values are reduced by 10% - 15%. We have verified (results not shown) that when decoherence is *absent*, the difference between I-V curves at low and high temperatures is negligible, indicating that thermal smearing is not responsible for PVR reduction observed in experiments.

To better interpret the experimental measurements, we include the electron-phonon scattering in top and bottom AGNR within the NEGF framework as shown in Eq. (3-4). Depending on different mechanisms, scattering can be elastic (acoustic phonon) and inelastic (optical phonon): $\mathbf{\Sigma}_{ph}^{r,<,>} = \mathbf{\Sigma}_{el}^{r,<,>} + \mathbf{\Sigma}_{inel}^{r,<,>}$. Following the Born approximation [27], the scattering self-energies can be solved self-consistently with Green's function:

$$\mathbf{\Sigma}_{el}^{<,>} = D_{el}\mathbf{G}^{<,>} \tag{8}$$

$$\mathbf{\Sigma}_{inel}^{<} = D_{inel}\left\{\left[n_B(\hbar\omega)+1\right]\mathbf{G}^{<}(\varepsilon+\hbar\omega) + n_B(\hbar\omega)\,\mathbf{G}^{<}(\varepsilon-\hbar\omega)\right\} \tag{9}$$

$$\mathbf{\Sigma}_{inel}^{>} = D_{inel}\left\{\left[n_B(\hbar\omega)+1\right]\mathbf{G}^{>}(\varepsilon-\hbar\omega) + n_B(\hbar\omega)\,\mathbf{G}^{>}(\varepsilon+\hbar\omega)\right\} \tag{10}$$

$$\mathrm{Im}\left[\mathbf{\Sigma}_{ph}^{r}\right] = \left[\mathbf{\Sigma}_{ph}^{>} - \mathbf{\Sigma}_{ph}^{<}\right]/2i \tag{11}$$

Here, n_B is the Boltzmann distribution; $\hbar\omega$ is the phonon energy; and D_{el} and D_{inel} are the electron-phonon deformation potentials. This model characterizes the scattering of electrons by three parameters, which are determined to satisfy the experimentally measurable electron mean free path in graphene: $D_{el} = 0.01\mathrm{eV}^2$, $D_{inel} = 0.07\mathrm{eV}^2$ and $\hbar\omega = 180\mathrm{meV}$ [28]. Phenomenologically, larger deformational potentials reflect stronger electron-phonon scattering, thus shorter electron mean free path. The mean free path obtained from our calculations is about $1.42\mu m$, consistent with the measured mean free path of graphene deposited on hBN substrate [29] (around $1.5\mu m$).

The simulation results with electron-phonon scattering are plotted in Fig. 4 (dashed lines). For the twisted heterostructures, the phonon-mediated current as a function of drain voltage preserves the NDR features. The PVR decreases compared to the case of coherent tunneling, whereas the magnitude of both peak and valley current is larger. When electron-phonon scattering exists, the conservation of wavevectors required for the tunneling of electrons between the two layers is weakened, resulting in the rise of tunneling current.

The reduction of PVR values observed in experiment is clearly captured in our simulation. In Fig. 4 inset, we plot the PVR values of the current peaks as a function of rotation angle in the coherent case and with phonon-scattering, where a 15% - 25% reduction of PVR values is observed. Therefore, the modeled results are in a reasonable agreement with the observations in experiments, demonstrating that the suppression of NDR features introduced by higher temperature is mainly due to a stronger decoherence mechanism including electron-phonon scattering.

IV. Conclusions

In summary, we model the electron transport properties of a three-terminal tunnel-FET device built with twisted graphene layers sandwiching hBN barrier. Robust NDR features in I-V characteristics are captured by the numerical simulation and distinct mechanisms are responsible for the resonant tunneling. The Fabry-Pérot like quantum interference vanishes at larger twisting angles. NDR peaks arising in the case of twisted graphene layers are controllable by both gate voltage and twisting angle. Analytical equations for V_b^R and V_b^P are derived. Moreover, the role of phonon induced decoherence is also numerically simulated to capture the effects of temperature increase in experiments. In the case of twisted graphene sheet, the NDR survives electron-phonon scattering but the peak-to-valley ratios are slightly reduced, consistent with experimental works.

REFERENCES

[1] L. Britnell, R. V. Gorbachev, R. Jalil, B. D. Belle, F. Schedin, M. I. Katsnelson, L. Eaves, S. V. Morozov, A. S. Mayorov, N. M. R. Peres, A. H. C. Neto, J. Leist, A. K. Geim, L. A. Ponomarenko, and K. S. Novoselov, "Electron tunneling through ultrathin boron nitride crystalline barriers," *Nano Lett.*, vol. 12, no. 3, pp. 1707–1710, 2012, doi: 10.1021/nl3002205.

[2] S. Bruzzone, D. Logoteta, G. Fiori, and G. Iannaccone, "Vertical transport in graphene-hexagonal boron nitride heterostructure devices," *Sci. Rep.*, vol. 5, Sep. 2015, Art. no. 14519, doi: 10.1038/srep14519.

[3] C. Dean, A. Young, L. Wang, I. Meric, G.-H. Lee, K. Watanabe, T. Taniguchi, K. Shepard, P. Kim, and J. Hone, "Graphene based heterostructures," *Solid State Commun.*, vol. 152, pp. 1275–1282, Aug. 2012, doi: 10.1016/j.ssc.2012.04.021.

[4] T. Georgiou, R. Jalil, B. D. Belle, L. Britnell, R. V. Gorbachev, S. V. Morozov, Y.-J. Kim, A. Gholinia, S. J. Haigh, O. Makarovsky, L. Eaves, L. A. Ponomarenko, A. K. Geim, K. S. Novoselov, and A. Mishchenko, "Vertical field-effect transistor based on graphene–WS_2 heterostructures for flexible and transparent electronics," *Nature Nanotechnol.*, vol. 8, pp. 100–103, Dec. 2013, doi: 10.1038/nnano.2012.224.

[5] H. Wang, T. Taychatanapat, A. Hsu, K. Watanabe, T. Taniguchi, P. Jarillo-Herrero, and T. Palacios, "BN/graphene/BN transistors for RF applications," *IEEE Electron Device Lett.*, vol. 32, no. 9, pp. 1209–1211, Sep. 2011, doi: 10.1109/LED.2011.2160611.

[6] Y. Xu, Z. Guo, H. Chen, Y. Yuan, J. Lou, X. Lin, H. Gao, H. Chen, and B. Yu, "In-plane and tunneling pressure sensors based on graphene/hexagonal boron nitride heterostructures," *Appl. Phys. Lett.*, vol. 99, no. 13, p. 133109, 2011, doi: 10.1063/1.3643899.

[7] X. Zhong, R. G. Amorim, R. H. Scheicher, R. Pandey, and S. P. Karna, "Electronic structure and quantum transport properties of trilayers formed from graphene and boron nitride," *Nanoscale*, vol. 4, pp. 5490–5498, Jul. 2012, doi: 10.1039/C2NR31310C.

[8] F. Amet, J. R. Williams, A. G. F. Garcia, M. Yankowitz, K. Watanabe, T. Taniguchi, and D. Goldhaber-Gordon, "Tunneling spectroscopy of graphene-boron-nitride heterostructures," *Phys. Rev. B*, vol. 85, p. 073405, Feb. 2012, doi: 10.1103/PhysRevB.85.073405.

[9] S. A. Khorasani, "Tunable spontaneous emission from layered graphene/dielectric tunnel junctions," *IEEE J. Quantum Electron.*, vol. 50, no. 5, pp. 307–313, May 2014, doi: 10.1109/JQE.2014.2308976.

[10] L. Britnell, R. M. Ribeiro, A. Eckmann, R. Jalil, B. D. Belle, A. Mishchenko, Y.-J. Kim, R. V. Gorbachev, T. Georgiou, S. V. Morozov, A. N. Grigorenko, A. K. Geim, C. Casiraghi, A. H. C. Neto, and K. S. Novoselov, "Strong light-matter interactions in heterostructures of atomically thin films," *Science*, vol. 340, no. 6138, pp. 1311–1314, 2013, doi: 10.1126/science.1235547.

[11] L. Britnell, R. V. Gorbachev, A. K. Geim, L. A. Ponomarenko, A. Mishchenko, M. T. Greenaway, T. M. Fromhold, K. Novoselov, and L. Eaves, "Resonant tunnelling and negative differential conductance in graphene transistors," *Nature Commun.*, vol. 4, Apr. 2013, Art. no. 1794, doi: 10.1038/ncomms2817.

[12] A. Mishchenko, J. S. Tu, Y. Cao, R. V. Gorbachev, J. R. Wallbank, M. T. Greenaway, V. E. Morozov, S. V. Morozov, M. J. Zhu, S. L. Wong, F. Withers, C. R. Woods, Y.-J. Kim, K. Watanabe, T. Taniguchi, E. E. Vdovin, O. Makarovsky, T. M. Fromhold, V. I. Fal'ko, A. K. Geim, L. Eaves, and K. S. Novoselov, "Twist-controlled resonant tunnelling in graphene/boron nitride/graphene heterostructures," *Nature Nanotechnol.*, vol. 9, pp. 808–813, Sep. 2014, doi: 10.1038/nnano.2014.187.

[13] S. C. de la Barrera, Q. Gao, and R. M. Feenstra, "Theory of graphene-insulator-graphene tunnel junctions," *J. Vac. Sci. Technol. B.*, vol. 32, no. 4, p. 04E101, 2014, doi: 10.1116/1.4871760.

[14] L. Brey, "Coherent tunneling and negative differential conductivity in a graphene/h-BN/graphene heterostructure," *Phys. Rev. A*, vol. 2, p. 014003, Jul. 2014, doi: 10.1103/PhysRevApplied.2.014003.

[15] R. M. Feenstra, D. Jena, and G. Gu, "Single-particle tunneling in doped graphene-insulator-graphene junctions," *J. Appl. Phys.*, vol. 111, no. 4, p. 043711, 2012, doi: 10.1063/1.3686639.

[16] K. M. M. Habib, F. Zahid, and R. K. Lake, "Negative differential resistance in bilayer graphene nanoribbons," *Appl. Phys. Lett.*, vol. 98, no. 19, p. 192112, 2011, doi: 10.1063/1.3590772.

[17] N. Mori, T. Edagawa, Y. Kamakura, and L. Eaves, "Nonequilibrium green function simulations of graphene-nanoribbon resonant-tunneling transistors," *Jpn. J. Appl. Phys.*, vol. 53, no. 4S, p. 04EN04, 2014, doi: 10.7567/JJAP.53.04EN04.

[18] B. Sensale-Rodriguez, "Graphene-insulator-graphene active plasmonic terahertz devices," *Appl. Phys. Lett.*, vol. 103, no. 12, p. 123109, 2013, doi: 10.1063/1.4821221.

[19] F. T. Vasko, "Resonant and nondissipative tunneling in independently contacted graphene structures," *Phys. Rev. B*, vol. 87, p. 075424, Feb. 2013, doi: 10.1103/PhysRevB.87.075424.

[20] Y. Zhao, Z. Wan, X. Xu, S. R. Patil, U. Hetmaniuk, and M. P. Anantram, "Negative differential resistance in boron nitride graphene heterostructures: Physical mechanisms and size scaling analysis," *Sci. Rep.*, vol. 5, May 2015, Art. no. 10712, doi: 10.1038/srep10712.

[21] P. Moon and M. Koshino, "Electronic properties of graphene/hexagonal-boron-nitride Moiré superlattice," *Phys. Rev. B*, vol. 90, p. 155406, Oct. 2014, doi: 10.1103/PhysRevB.90.155406.

[22] G. T. de Laissardière, D. Mayou, and L. Magaud, "Localization of dirac electrons in rotated graphene bilayers," *Nano Lett.*, vol. 10, no. 3, pp. 804–808, 2010, doi: 10.1021/nl902948m.

[23] J. Gaskell, L. Eaves, K. S. Novoselov, A. Mishchenko, A. K. Geim, T. M. Fromhold, and M. T. Greenaway, "Graphene-hexagonal boron nitride resonant tunneling diodes as high-frequency oscillators," *Appl. Phys. Lett.*, vol. 107, no. 10, p. 103105, 2015, doi: 10.1063/1.4930230.

[24] M. Anantram, M. S. Lundstrom, and D. E. Nikonov, "Modeling of nanoscale devices," *Proc. IEEE*, vol. 96, no. 9, pp. 1511–1550, Sep. 2008, doi: 10.1109/JPROC.2008.927355.

[25] U. Hetmaniuk, Y. Zhao, and M. P. Anantram, "A nested dissection approach to modeling transport in nanodevices: Algorithms and applications," *Int. J. Numer. Methods Eng.*, vol. 95, pp. 587–607, Aug. 2013, doi: 10.1002/nme.4518.

[26] M. T. Greenaway, E. E. Vdovin, A. Mishchenko, O. Makarovsky, A. Patane, J. R. Wallbank, Y. Cao, A. V. Kretinin, M. J. Zhu, S. V. Morozov, V. I. Fal'ko, K. S. Novoselov, A. K. Geim, T. M. Fromhold, and L. Eaves, "Resonant tunnelling between the chiral Landau states of twisted graphene lattices," *Nature Phys.*, vol. 11, pp. 1057–1062, Oct. 2015, doi: 10.1038/nphys3507.

[27] A. Svizhenko and M. P. Anantram, "Effect of scattering and contacts on current and electrostatics in carbon nanotubes," *Phys. Rev. B*, vol. 72, p. 085430, Aug. 2005, doi: 10.1103/PhysRevB.72.085430.

[28] N. D. Akhavan, G. Jolley, G. A. Umana-Membreno, J. Antoszewski, and L. Faraone, "Phonon limited transport in graphene nanoribbon field effect transistors using full three dimensional quantum mechanical simulation," *J. Appl. Phys.*, vol. 112, no. 9, p. 094505, 2012, doi: 10.1063/1.4764318.

[29] A. S. Mayorov, R. V. Gorbachev, S. V. Morozov, L. Britnell, R. Jalil, L. A. Ponomarenko, P. Blake, K. S. Novoselov, K. Watanabe, T. Taniguchi, and A. K. Geim, "Micrometer-scale ballistic transport in encapsulated graphene at room temperature," *Nano Lett.*, vol. 11, no. 6, pp. 2396–2399, 2011, doi: 10.1021/nl200758b.